

HIGH-SPEED RAILWAY TRACKS OF A SURFACE, BRIDGE AND TUNNEL LINE AND SOME EFFECTS ON THE TRAIN-INDUCED BRIDGE AND GROUND VIBRATIONS

Lutz Auersch¹

¹ Federal Institute for Materials Research and Testing,
D 12200 Berlin, Germany
e-mail: lutz.auersch-saworski@bam.de

Keywords: Track compliance, surface line, bridge track, tunnel track, ground vibration, layered soil, bridge resonance, train speed, axle sequence, track irregularities.

Abstract. *Different high-speed railway tracks have been analysed theoretically and experimentally, a ballasted track at a surface line, a slab track in a tunnel, and a ballasted track on a concrete bridge. Vehicle, track and ground vibration as well as their interaction are considered in a combined finite-element boundary-element (FEBEM) approach. The layered soil is calculated in frequency wavenumber domain and the solution for fixed or moving point or track loads follow as wavenumber integrals. The comparison of the dynamic compliances of the different tracks leads to an improved understanding of the different track elements. Certain maxima have been observed for certain train speeds and certain eigenmodes of the bridge. These maxima correlate with some maxima of the ground vibrations. The bridge and the ground vibrations are discussed with the axle-sequence of the train. The ground vibrations strongly depend on the regular and random inhomogeneity of the soil. The regular layering of the soil yields a cut-on and resonance phenomenon whereas the random inhomogeneity yields a scattering of the axle impulses which proved to be important for high-speed trains. All theoretical results are compared with measurements at a high-speed line.*

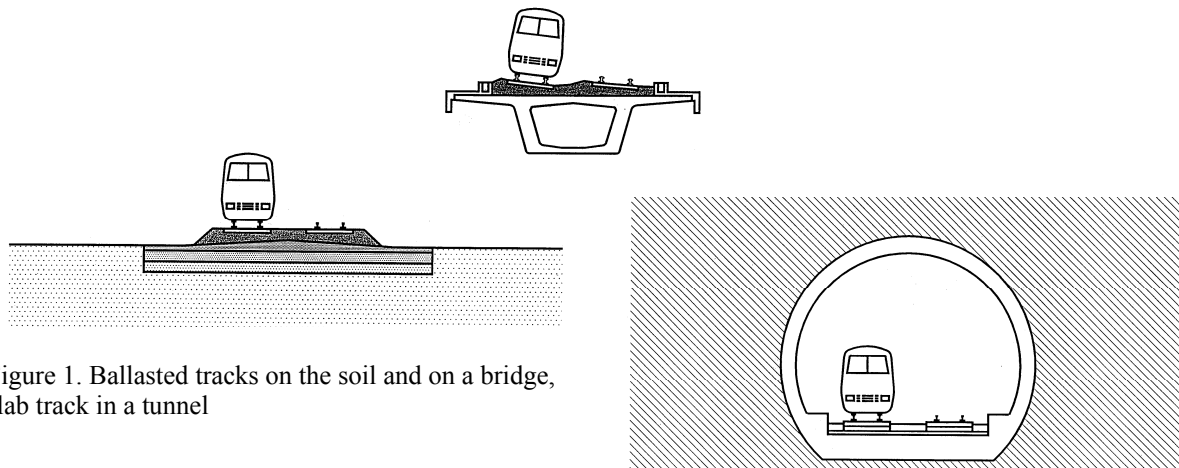


Figure 1. Ballasted tracks on the soil and on a bridge, slab track in a tunnel

1 FINITE-ELEMENT BOUNDARY ELEMENT METHOD FOR THE DYNAMIC COMPLIANCE OF TRACKS ON LAYERED SOILS

A 3-dimensional track model is combined with the boundary element formulation of the soil. That means, that the Greens' functions of a homogeneous or layered soil are used to establish a fully coupling soil matrix which is added to the FEM matrix of the track.

1.1 Green's functions of the soil

The soil is a homogeneous or horizontally layered elastic half-space, which is excited at its surface by dynamic forces \mathbf{F} , and the displacements \mathbf{u} have to be calculated for surface points, too. The relation between the displacements \mathbf{u} and the force \mathbf{F} can be described in cylindrical (transversal, radial and vertical) components as

$$\begin{bmatrix} u_t \\ u_r \\ u_z \end{bmatrix} = \begin{bmatrix} f_{tt} & 0 & 0 \\ 0 & f_{rr} & f_{rz} \\ 0 & -f_{rz} & f_{zz} \end{bmatrix} \begin{bmatrix} F_t \\ F_r \\ F_z \end{bmatrix} \quad (1)$$

The four functions $f_{ij}(r, \omega)$ of distance and circular frequency can be calculated by integration in wavenumber domain [1], for example as

$$f_{zz} = \frac{1}{2\pi} \int_0^{\infty} H_{zz}(k) J_0(kr) k dk \quad (2)$$

for the simplest case of the vertical component. J_0 is the Bessel function of the first kind and the vertical compliance H_{zz} in wavenumber domain k can be given explicitly for the homogeneous half-space

$$H_{zz} = \frac{k_s^2 \sqrt{k_p^2 - k^2}}{iG \left[(k_s^2 - 2k^2)^2 + 4k^2 \sqrt{k_s^2 - k^2} \sqrt{k_p^2 - k^2} \right]} \quad (3)$$

with the abbreviations (v_s, v_p the shear and compressional wave velocities)

$$k_s = \omega / v_s \quad k_p = \omega / v_p \quad (4)$$

or calculated by matrix methods for a layered soil [1, 2]. Similar formulas hold for the other components and the complete set of Green's functions (1) is used in the present boundary element method of the soil.

1.2 The stiffness matrix of the discretized soil

First, the soil has to be defined by a set of m surface points with coordinates \mathbf{x}_α . A certain portion A_α of the surface area belongs to each surface point. A force \mathbf{F} at a point \mathbf{x}_α of the surface of the soil is considered. By using the Green's functions (of the preceding section), the displacements at all other points \mathbf{x}_β are calculated

$$\begin{bmatrix} u_x \\ u_y \\ u_z \end{bmatrix} = \begin{bmatrix} f_{rr} x_r^2 + f_{tt} y_r^2 & (f_{rr} - f_{tt}) x_r y_r & f_{rz} x_r \\ (f_{rr} - f_{tt}) x_r y_r & f_{rr} y_r^2 + f_{tt} x_r^2 & f_{rz} y_r \\ -f_{rz} x_r & -f_{rz} y_r & f_{zz} \end{bmatrix} \begin{bmatrix} F_x \\ F_y \\ F_z \end{bmatrix} \quad (5)$$

with

$$x_r = (x_\alpha - x_\beta) / r \quad y_r = (y_\alpha - y_\beta) / r$$

Equation (5) is the same as equation (1), but transformed into the cartesian coordinate system.

For the point of excitation \mathbf{x}_α itself, the Green's function cannot be evaluated because the solution is singular at this point. This difficulty can be overcome by calculating the mean value over the corresponding surface area. This leads to the mean values of the scalar functions $f_{ii}(r)$

$$\bar{f}_{ii} = \frac{2}{r_\alpha^2} \int_0^{r_\alpha} f_{ii}(r) r dr \quad (6)$$

where r_α is the radius of area A_α . So the compliance relation at the excited point of the soil is

$$\begin{bmatrix} u_x \\ u_y \\ u_z \end{bmatrix} = \begin{bmatrix} \frac{\bar{f}_{rr} + \bar{f}_{tt}}{2} & 0 & 0 \\ 0 & \frac{\bar{f}_{rr} + \bar{f}_{tt}}{2} & 0 \\ 0 & 0 & \bar{f}_{zz} \end{bmatrix} \begin{bmatrix} F_x \\ F_y \\ F_z \end{bmatrix} \quad (7)$$

The flexibility matrix of the soil is assembled of all these 3x3 matrices $\mathbf{f}_{\beta\alpha}$

$$\begin{bmatrix} \mathbf{u}_1 \\ \vdots \\ \mathbf{u}_\beta \\ \vdots \\ \mathbf{u}_m \end{bmatrix} = \begin{bmatrix} \mathbf{f}_{11} & \cdots & \mathbf{f}_{1\alpha} & \cdots & \mathbf{f}_{1m} \\ \vdots & & \vdots & & \vdots \\ \mathbf{f}_{\beta 1} & \cdots & \mathbf{f}_{\beta\alpha} & \cdots & \mathbf{f}_{\beta m} \\ \vdots & & \vdots & & \vdots \\ \mathbf{f}_{m1} & \cdots & \mathbf{f}_{m\alpha} & \cdots & \mathbf{f}_{mm} \end{bmatrix} \begin{bmatrix} \mathbf{F}_1 \\ \vdots \\ \mathbf{F}_\alpha \\ \vdots \\ \mathbf{F}_m \end{bmatrix} \quad (8)$$

with m the number of points, or in short form

$$\mathbf{u} = \mathbf{f} \mathbf{F} \quad (8')$$

The inversion of this equation

$$\mathbf{F} = \mathbf{f}^{-1} \mathbf{u} =: \mathbf{K}_S \mathbf{u} \quad (9)$$

gives the dynamic stiffness matrix $\mathbf{K}_S = \mathbf{f}^{-1}$ of the soil which is introduced in the finite element procedure for the structure [3].

1.3 Combined finite-element boundary-element method

Now the coupling of both sub-systems, track and soil, is done by introducing the soil into the finite element code as a new type of element. The points of the soil define one special element of which the dynamic stiffness matrix \mathbf{K}_S is calculated by the boundary element method. The track structure is described by the conventional finite element method. Local stiffness matrices as well as local mass matrices are assembled in a global stiffness matrix \mathbf{K}_0 and a global mass matrix \mathbf{M} respectively. Combining these matrices, the frequency-dependent dynamic stiffness matrix $\mathbf{K}_F(\omega)$ of the track structure

$$\mathbf{K}_F = \mathbf{K}_0 - \omega^2 \mathbf{M} \quad (10)$$

is obtained. Then the coupling of the boundary element and finite element part of the system can be expressed in terms of global representations of the matrices and

$$\mathbf{F} = (\mathbf{K}_F(\omega) + \mathbf{K}_S(\omega)) \mathbf{u} \quad (11)$$

is the equation of the whole track-soil system, that has to be solved for given external forces \mathbf{F} , for example the wheel-set forces.

2 CALCULATED COMPLIANCES OF BALLASTED AND SLAB TRACKS

Three different tracks, a ballasted surface track, a ballast track on a bridge and a slab track in a tunnel are considered (Fig. 1). All tracks have the same UIC60 rails with bending stiffness $EI_R = 6.4 \cdot 10^6 \text{ Nm}^2$ and mass per length $m' = 60 \text{ kg/m}$, and the same concrete sleepers with $EI_S = 5.2 \cdot 10^6 \text{ Nm}^2$ and $m = 338 \text{ kg}$. For each track, the stiffness of the material under the track (the ballast or the subsoil of the slab) is varied.

2.1 Ballasted track on a homogeneous soil

The surface track consists of a 0.35 m ballast layer. The sub-soil has a shear wave velocity of $v_S = 300 \text{ m/s}$. The rail pads are rather stiff with $k_P = 300 \text{ kN/m}$. The ballast is varied as

$$v_S = 100, 150, 200, 300 \text{ m/s}.$$

The dynamic compliances of the rails are given as amplitude and phase in Figure 2. Although the ballast stiffness is varied by a factor of 9, the static compliance of the rail is in the narrow range of $u/P = 1.8$ to $3.2 \cdot 10^{-9} \text{ m/N}$. That means 0.2 to 0.3 mm displacement under a 100 kN axle load. The stiff ballast yields an almost constant compliance and only a small phase delay of 20° . All softer ballast materials result in a stronger phase delay and a related amplitude reduction at a certain frequency which is lower for the softer ballast. The softest ballast has a strong phase and amplitude decay at about 60 Hz. The softest ballast with $v_S = 100 \text{ m/s}$ has the strongest contrast with the underlying soil $v_S = 300 \text{ m/s}$ and this results in moderate amplifications of the track amplitudes.

2.2 Ballasted track on a bridge (rigid base)

The ballasted track is the same on the bridge as for the surface line. The bottom of the ballast layer is fixed. The same variation of the ballast stiffness is analysed in Figure 2b. The rigid base reduces the static compliances of the ballasted tracks to values between $u/P = 1.4$ to $2.9 \cdot 10^{-9} \text{ m/N}$. No radiation damping of the soil is present and only small phase values due to the material damping can be observed. Clear resonances occur for the softer ballast materials at $f = 95$ and 135 Hz for $v_S = 100$ and 150 m/s . These resonance frequencies are lower than the layer frequencies $f = v_P/4d = 200/1.4 = 140$ or $300/1.4 = 210 \text{ Hz}$ due to the influence of the track mass. The phase decay at the resonance is stronger than for the surface line.

2.3 Slab track in a tunnel (on a layer over bedrock)

The slab track in the tunnel has a 0.6 m thick concrete plate which lies on a 1.5 m layer of softer soil material. The base is the tunnel floor which is assumed to be rigid. Medium soft rail pads of $k_P = 60 \text{ kN/m}$ are used to compensate the stiff track plate. The compliance of the rail is ruled by these soft rail pads and is constant if the stiffness of the sub-soil is varied between $v_S = 100$ and 300 m/s . Moreover it does not change its static value of $u/P = 3.7 \cdot 10^{-9} \text{ m/N}$ with increasing frequency (see Fig. 2d). The influence of the sub-soil can be clearly seen for the plate compliance under the axle load (Fig. 2c). The massive plate yields low resonance frequencies of $f = 20, 30, 40$ and 60 Hz with the compliances of the different sub-soils. These resonance frequencies are far below the layer resonances at $f = 33, 50, 66$ and 100 Hz . The amplitudes of the plate are much smaller than those of the rail. It is 20 or 10 % for the soft sub-soils and even less for the stiff sub-soils.

Figure 2d shows the rail compliances of the three tracks, surface track with soft ballast, bridge track with soft ballast, and tunnel track with a thick plate over a stiff sub-soil. The rail compliance of the tunnel is increasing at 150 Hz, the end of the frequency range. The resonance of the rail on the soft rail pads is expected at 205 Hz. While the ballasted tracks show a

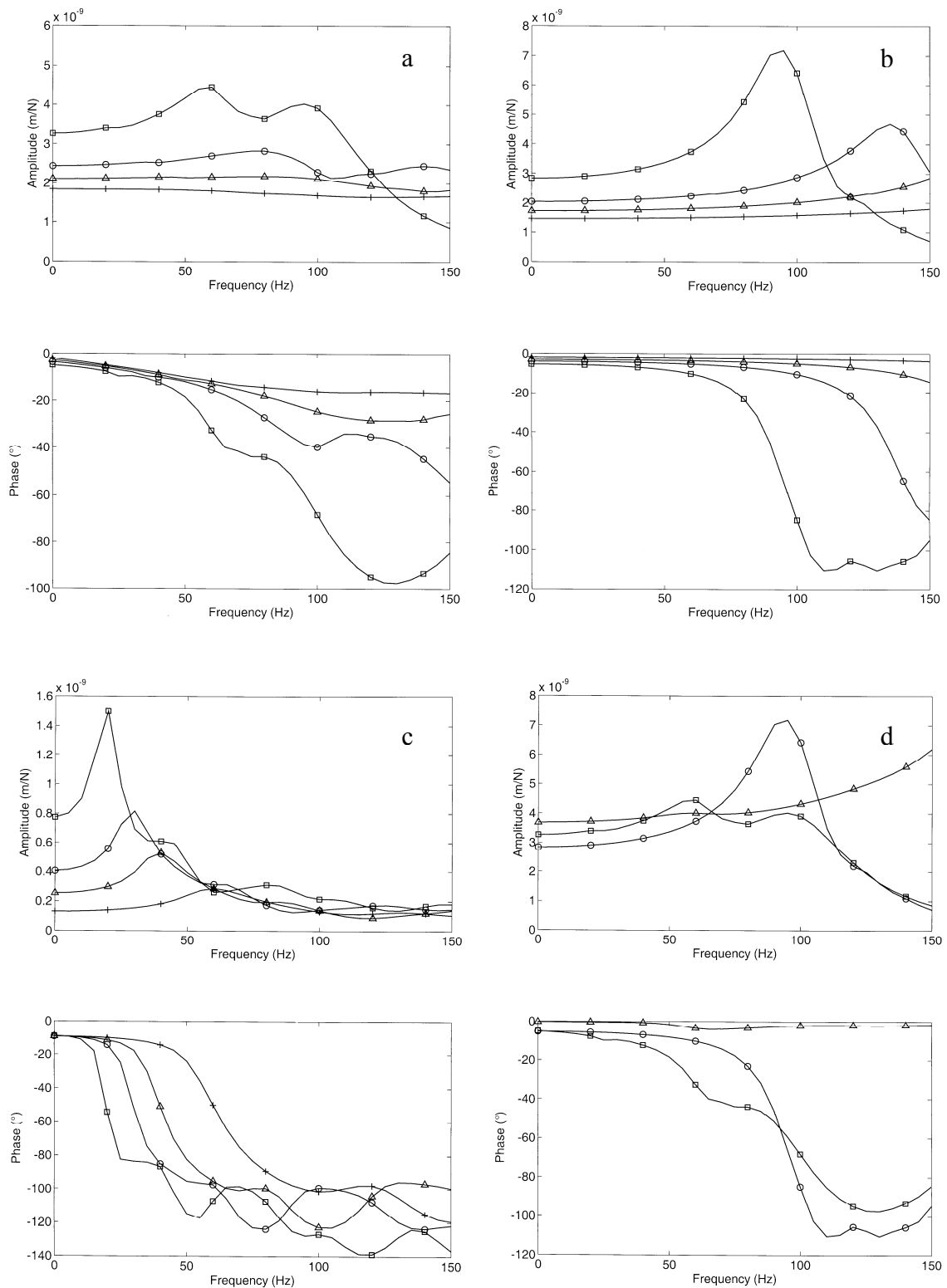


Figure 2: Compliances of different tracks, a) ballasted track on the soil, b) ballasted track on the bridge, c) slab track on a sub-soil layer (compliance of the plate) variation of the ballast or subsoil \square 100, \circ 150, \triangle 200 +300 m/s in a, b, c. Comparison of the rail compliances (d) for the ballasted track on the soil \square , the ballasted track on the bridge \circ , and the slab track \triangle .

phase drop below 100 Hz, the rail of the tunnel track shows almost no phase delay. Such strong differences between rail and sleeper displacements are only found for the tunnel track. The sleeper to rail displacement ratio of the ballasted tracks is at 33 to 67 % for the bridge track line and at 50 to 77 % for the surface line. The differences increase with a stiffer ballast material, but also with a softer rail pad.

3 TRAIN INDUCED GROUND VIBRATION

3.1 Calculation in wavenumber domain

An alternative method to the FEBEM is the calculation of an infinite track in frequency-wavenumber domain. This method yields the track behaviour and the ground vibration due to moving or fixed loads [4]. The dynamic stiffness of the soil under the track in frequency wavenumber domain is calculated as the wavenumber integral

$$H(k_y, \omega) = \frac{1}{2\pi} \int_{-\infty}^{+\infty} H(k_x, k_y, \omega) p_1(k_x) dk_x = \frac{1}{K_S(k_y, \omega)} \quad (12)$$

The dynamic stiffness K_S of the soil is combined with the stiffness $K_T = EI k^4 - m' \omega^2$ of the track

$$H_{TS}(k_y, \omega) = \frac{1}{K_T + K_S} \quad T_{TS}(k_y, \omega) = \frac{K_S}{K_T + K_S} \quad (13)$$

and these track-soil transfer functions are used to calculate the displacements of the track and the soil

$$u_T(\omega) = \frac{F}{2\pi} \int_{-\infty}^{+\infty} H_{TS}(k_y, \omega - k_y v) dk_y \quad (14)$$

$$u_S(x, y^*, \omega) = \frac{F}{(2\pi)^2} \int_{-\infty}^{+\infty} \int_{-\infty}^{+\infty} H(k_x, k_y, \omega - k_y v) T_{TS}(k_y, \omega - k_y v) p_1(k_x) e^{i(k_x x + k_y y^*)} dk_x dk_y$$

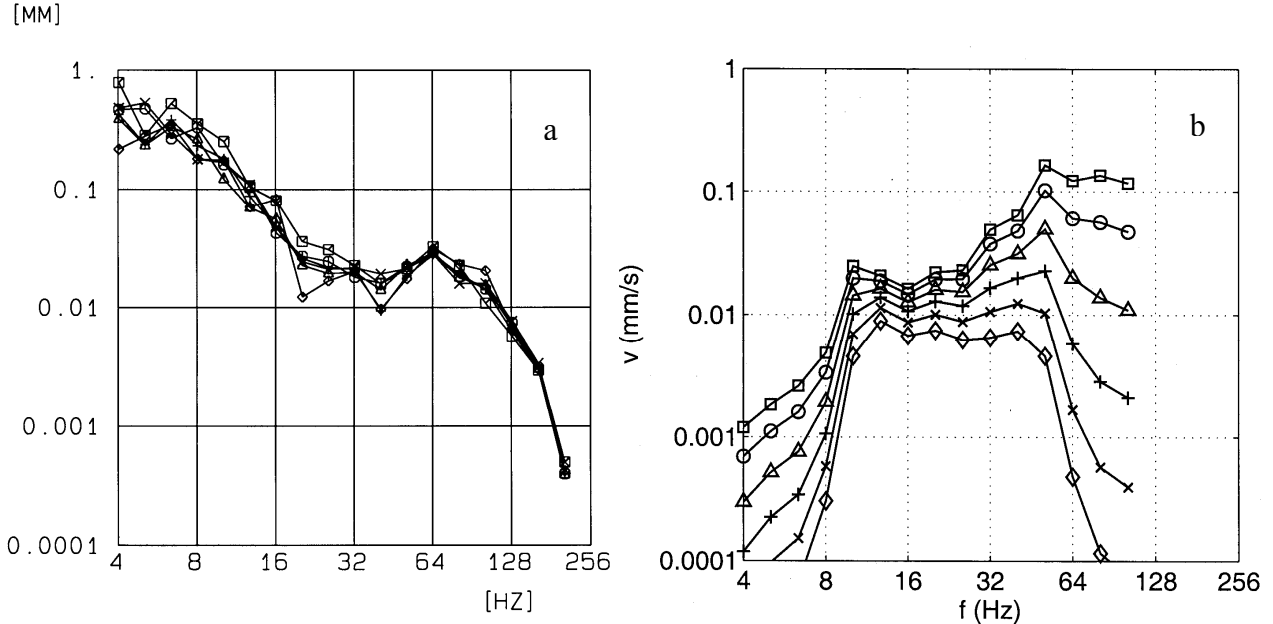


Figure 3: a) Third-of-octave spectra of the irregularities of the ballasted track at six different places of the 3 km long testing section; b) calculated ground vibration at the layered site; at \square 2.5, \circ 7.5, \triangle 12.5, $+$ 20, \times 30, \diamond 50 m distance from the track.

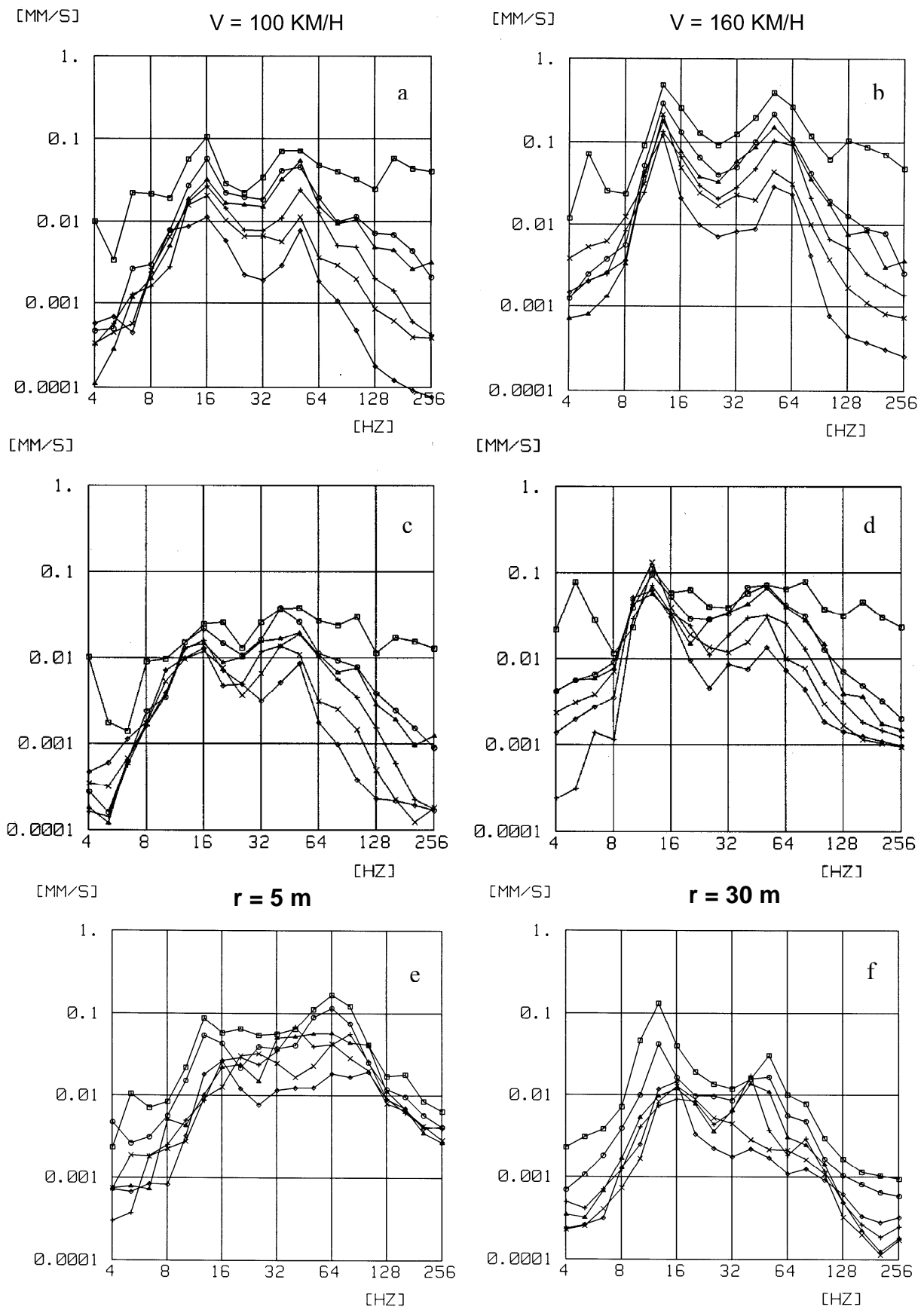


Figure 4: Train induced ground vibration, a), b) passage of a locomotive with $v_T = 100$ and 160 km/h , c), d) passage of a passenger car with $v_T = 100$ and 160 km/h , measured at \square 2.5, \circ 7.5, \triangle 12.5, $+$ 20, \times 30, \diamond 50 m, e), f) results at $r = 5$ and 30 m with train speeds $v_T = \square$ 160, \circ 125, \triangle 100, $+$ 80, \times 63, \diamond 40 km/h .

The spectrum of vibration amplitudes $v(x, \omega)$ at a fixed point for an excitation frequency ω_E is calculated as [5]

$$v(x, \omega, \omega_E) = \frac{F}{2\pi v_T} T_{BS}\left(\frac{\omega_E - \omega}{v_T}, \omega\right) \int_{-\infty}^{+\infty} H(k_x, \frac{\omega_E - \omega}{v_T}, \omega) p_1(k_x) \exp(ik_x x) dk_x. \quad (15)$$

The excitation of the ground vibration is a force spectrum $F(\omega)$ which is due to the irregularities s of the track. The irregularity spectrum $s(\omega)$ of the ballasted track is shown in Figure 3a for different places of the 3 km long test section. The soil consists of a layer with $v_s = 250$ m/s and $h = 10$ m on a rock half-space of $v_s = 1000$ m/s. The material damping of the soil is increasing from $D = 1\%$ at 10 Hz to $D = 10\%$ at 100 Hz, see [6] for more details. The calculated response of the soil is shown in Figure 3b for distances between 2.5 to 50 m.

While the irregularities are decreasing with frequency, the resulting excitation forces are almost constant, and the ground vibration amplitudes are mainly increasing with frequency. There is a strong cut-off for the frequencies below 12.5 Hz, which is the resonance frequency of the soil layer. The increase of the amplitudes is very strong below the cut-off, and moderate above. Frequencies above 63 Hz are reduced considerably due to the strong material damping. The two cut-off phenomena yield a specific frequency range of the ground vibration between 10 and 63 Hz which is due to the soil and not to the train excitation. All these theoretical characteristics are in good agreement with the experimental results in Figure 4c.

3.2 Experimental observations

The measured ground vibrations of different distances, different train speeds and different trains are shown on Figure 4, [7] where the spectra due to the locomotive display stronger and clearer characteristics than those of the passenger cars. A sharp resonance is observed for the layer frequency at 12.5 Hz in case of a train speed of 160 km/h. The same excitation frequency would be at 8 Hz for the lower train speed of $v_T = 100$ km/h, but no resonance is observed. The frequency is in the cut-off region of the soil, and therefore only small amplifications can be seen in the near field which indicate some specific train excitation. The characteristics of the layered and strongly damped soil are so dominant that the spectra of the different train speeds (Fig. 4e and f) are very similar. At a near-field distance of 5 m, the characteristic frequency range from 10 to 63 Hz has an almost constant level whereas the low frequencies are more dominant in the far field at 30 m. An increase of the amplitudes with increasing train speed can be observed. Especially the increase for $v_T = 160$ km/h due to the resonance at $f = 12.5$ Hz is very strong in the far field.

4 TRAIN INDUCED BRIDGE VIBRATION

4.1 Experimental observations

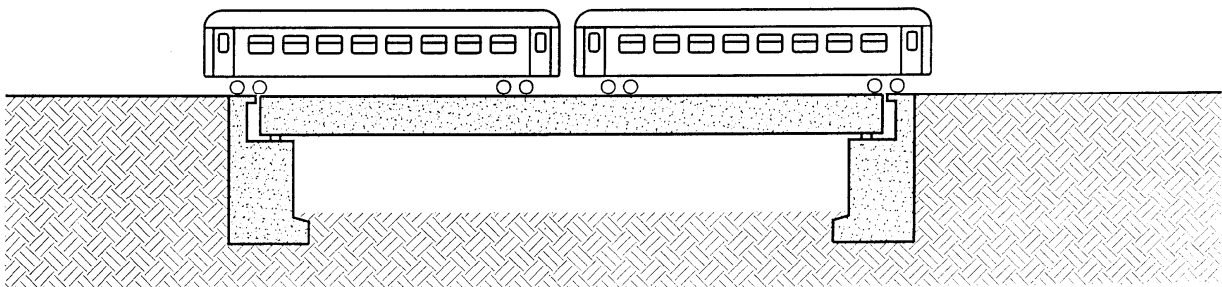


Figure 5: 45 m long concrete bridge on elastic bearings

A 45 m long concrete bridge has been analysed and measured (Fig. 5), [7]. The cross section can be seen on Figure 1. The bridge is simply supported on elastic bearings. The first four modes and eigenfrequencies are shown on Figure 6. The first bending mode fits perfectly the mode shape of a simply supported bridge. The first torsional mode has a contribution of the elastic bearings. During the passage of the test train, a clear excitation of the 7 Hz resonance has been observed for a train speed of $v_T = 100$ km/h and of the 11 Hz resonance for $v_T = 160$ km/h (see Figure 11 in Appendix A), [7]. These frequencies are close to those observed on the soil.

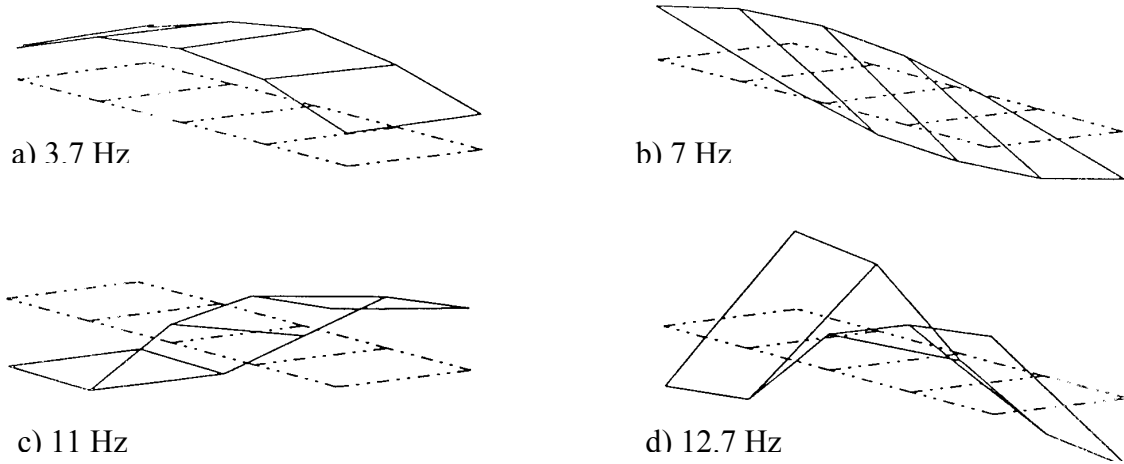


Figure 6: The first four eigenmodes of the concrete railway bridge a) first bending mode, b) first torsional mode, c) second bending mode, d) second torsional mode.

4.2 Modal excitation of railway bridges by sequence of axle loads

To examine the effect of passing trains, first a single axle passage over the bridge is considered. (The moving load concept is used here which is conservative compared to the more detailed train-bridge interaction, see for example [8]).

The excitation of mode j with circular eigenfrequency ω_j and normalized eigenform $v_j(x)$ can be determined from the Fourier transformed differential equation of this mode

$$m_j(\omega_j^2 + 2Di\omega_j^2 - \omega^2)u_j = F_j(\omega) \quad (16)$$

where

$$F_j(\omega) = \text{FFT}\{F(t)v_j(x = v_T t)\} \quad (17)$$

is the transformed modal force component. The static load F_S yields

$$F_j(\omega) = F_S \text{FFT}\{v_j(x = v_T t)\} = F_S V_j(\omega) \quad (18)$$

and a harmonic dynamic load F_D of frequency ω_j yields

$$F_j(\omega_j) \approx F_D V_j(0). \quad (19)$$

Figure 8 shows the forces of the first and second mode as time histories and spectra. The low frequencies have always high amplitudes which are related to the slow impulse of the total passage of the static force. These frequencies are much lower than the resonance frequencies of the bridge. A resonance due to the bridge passage impulse is only possible for the high-speed passage over a short bridge.

The higher frequencies are due to the irregularities when the static load is entering and leaving the bridge. The simply supported bridge yields a sudden bend at the beginning of the bridge. If the bridge is on an elastic support, as in the present situation, there is an additional step. Both cases, the simply supported bridge on a rigid or elastic support are shown in Figure

8. The additional step of 15 % of the maximum displacement for the elastic support yields high-frequency amplitudes which are up to five times higher than for the bridge on rigid support. There is a strong variation with frequency due to the constructive or destructive superposition of the entering and leaving of the bridge. As the resonance curve has some bandwidth, a smoothed curve of the modal force $F_j(\omega)$ is better suited to discuss possible resonances.

Another excitation of the bridge is due to the irregularities s of the track. The measured irregularities of the ballasted track on the bridge are shown in Figure 7a. From the irregularities at the resonance frequencies 7 and 11 Hz, $s = 2$ and 1 mm, dynamic forces of approximately $F_7 = F_{11} = 1$ kN are deduced. Their effects on the modes of the bridge are shown in Figure 8c and d. The amplitudes of the modal forces are almost the same as the amplitudes due to the entering and leaving of the simply supported bridge (Fig. 8a and 8b).

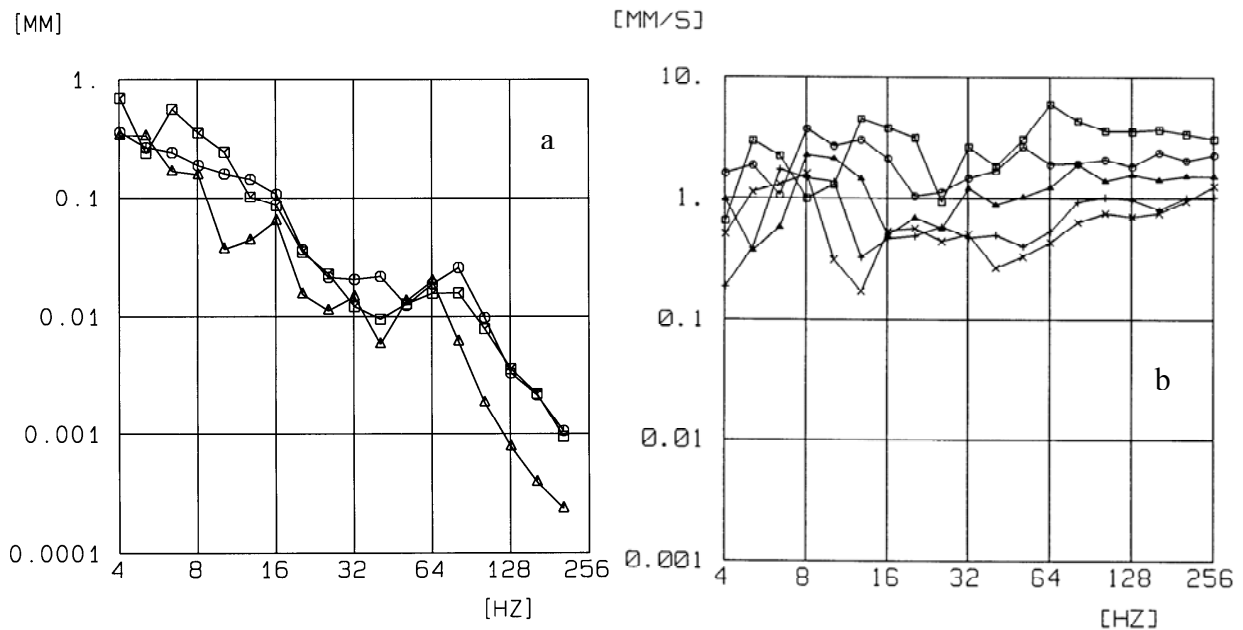


Figure 7: a) Irregularities of the track □ on the soil, ○ on the bridge, △ in the tunnel (slab track),
b) vibration spectra of the bridge track during the passage of the passenger car with
 $v_T = \square 160, \circ 125, \triangle 100, + 80, \times 63$ km/h.

So far, no reason for the different excitation of different modes could be found. It should be due to the specific axle sequence of the train which is shown on Figure 9 for the two interesting train speeds and on Figure 7b in a third-of-octave version for all train speeds. A maximum is found at 7 Hz for 100 km/h and at 11 Hz for 160 km/h close to the excited eigenfrequencies. Each maximum is the highest peak in a wider frequency band with several peaks. At the same time there are minima and a range of reduced amplitudes around 7 Hz for the train speed of 160 km/h and around 11 Hz for 100 km/h. Moreover, these minima are also found for a single car or a single locomotive (Fig. 9c-d). So it is concluded, that the axle sequence is important for the excitation of the eigenfrequencies of the bridge. The axle sequence yields maxima and minima which are suitable to the experimental observation, and the cancellation due to the sequence of the axles seems to be more important [9]. Isolated peaks of the axle sequence spectrum are only found for specific, very regular trains [10].

The axles-sequence spectra discussed here are in relation to the signatures of trains in the UIC rules [11] which are expressed as the axle loads as a function of the wave length. But the axle sequence spectra also include higher frequencies which are important for the train-bridge situation discussed here.

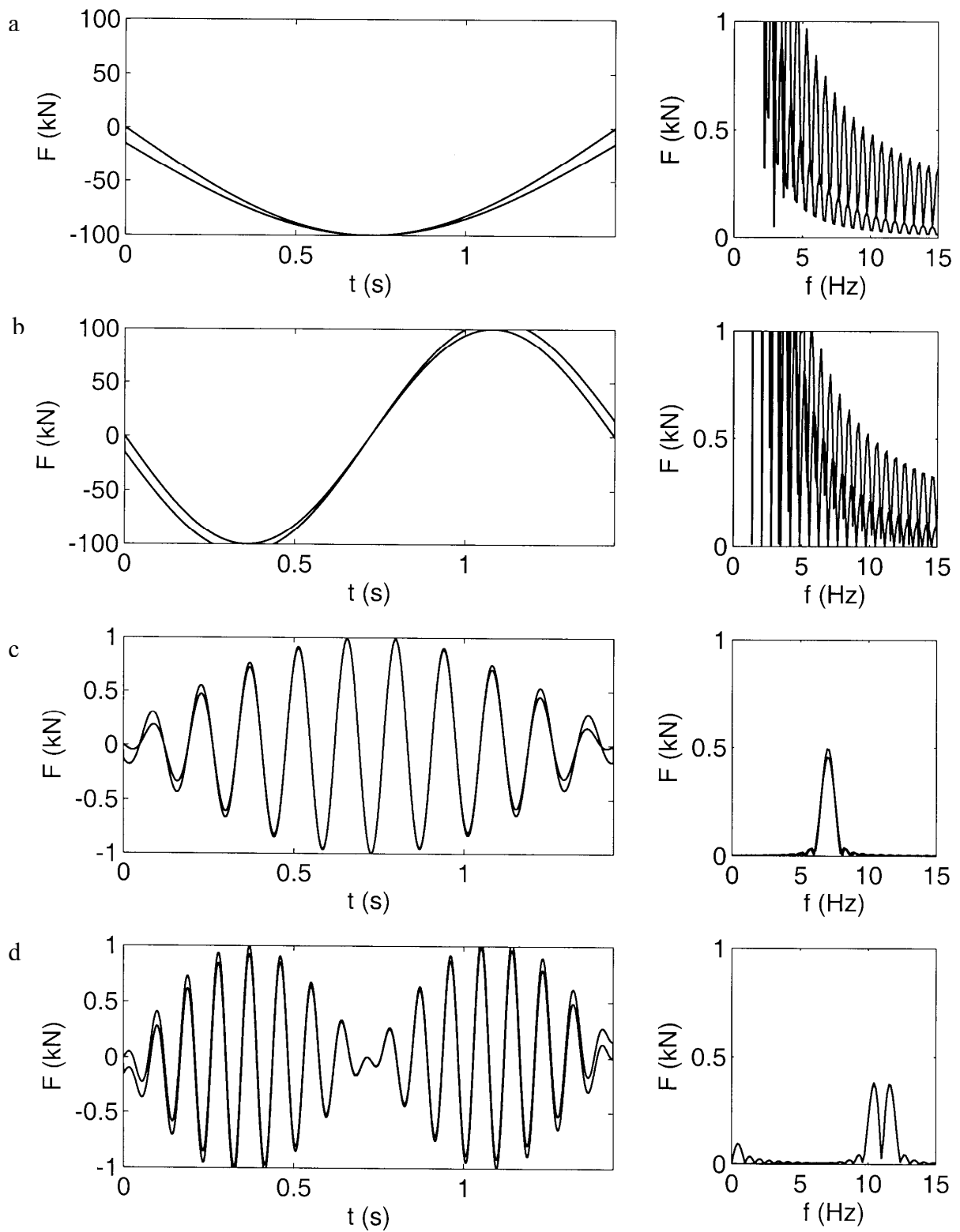


Figure 8: Modal forces as time history and spectra, due to the passage of a static load, a) first and b) second mode, and due to harmonic loads of $f =$ c) 7 Hz for the first mode and d) 11 Hz for the second mode, all results are given for rigid and elastic support.

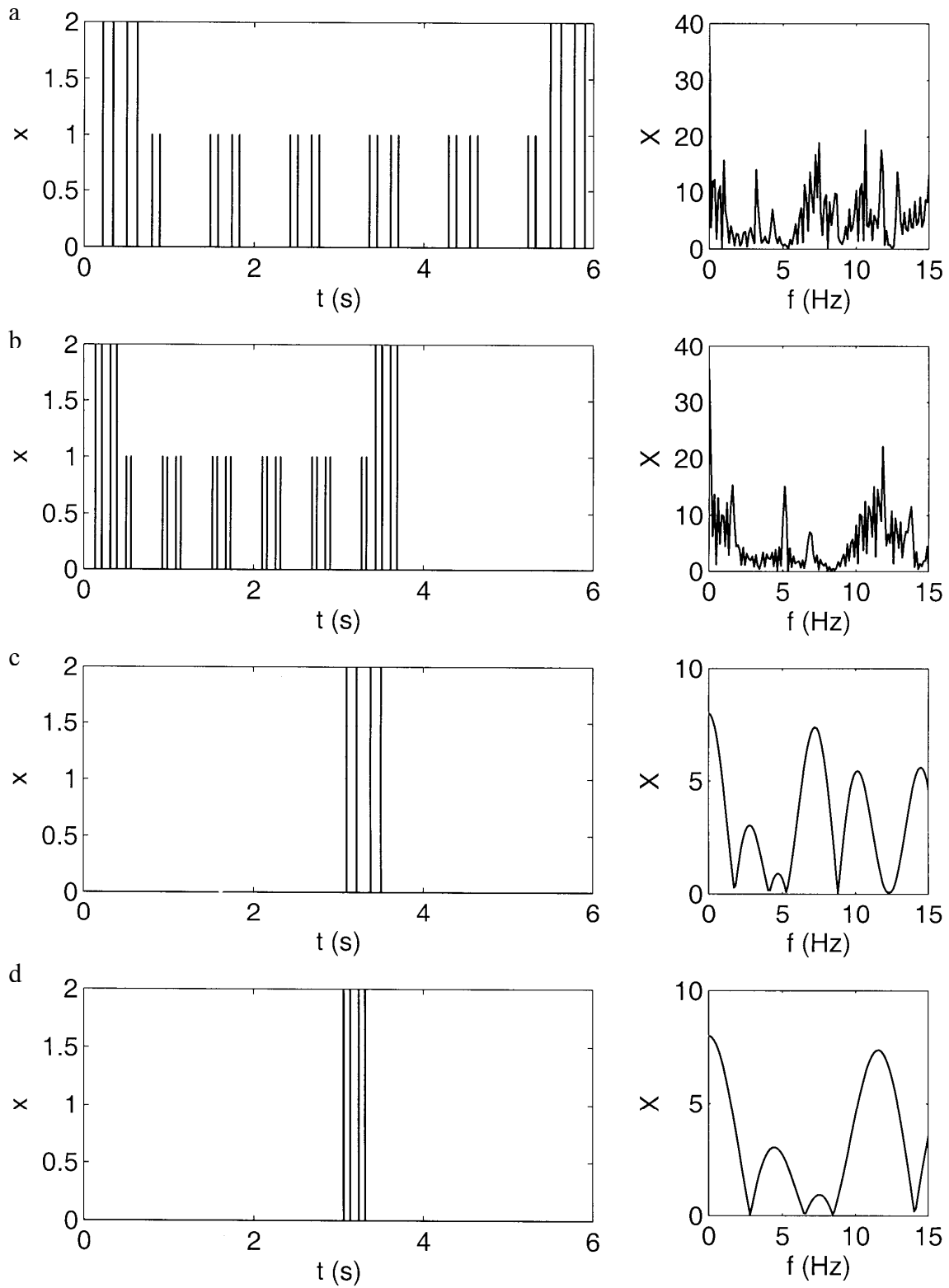


Figure 9: Axles sequence of the test train with $v_T =$ a) 100 and b) 160 km/h, time histories and spectra, c) and d) of the locomotive with 100 and 160 km/h respectively.

5 CONCLUSIONS

- The calculated compliances of different ballasted and slab tracks on layered soils show some typical characteristics, resonances, amplitude and phase delays, rail to sleeper amplitude ratios, which can also be found in the measurements.
- Dominant frequencies, which have been measured on the ground, are close to the resonance frequencies of the bridge that are excited by trains of the same speed.
- The excitation of the modes of the bridge can be due to the passing over the bridge, the entering and leaving of the bridge or the random irregularities of the track.
- All these excitations are modified by the axle sequence of the whole train. In the present case the axle sequence spectrum has a maximum at the excited eigenfrequency and a minimum at the other eigenfrequency of the bridge.
- The maximum of the axle sequence spectrum also excites the layer resonance of the soil for a train speed of 160 km/h whereas the same excitation is in the cut-off region of the soil for a train speed of 100 km/h.

REFERENCES

- [1] L. Auersch, Wave propagation in layered soil: theoretical solution in wavenumber domain and experimental results of hammer and railway traffic excitation. *Journal of Sound and Vibration*, **173**, 233-264, 1994.
- [2] L. Auersch, Wave propagation in the elastic half-space due to an interior load and its application to ground vibration problems and buildings on pile foundations. *Soil Dynamics and Earthquake Engineering*, **30**, 925-936, 2010.
- [3] L. Auersch, Dynamics of the railway track and the underlying soil: the boundary-element solution, theoretical results and their experimental verification. *Vehicle System Dynamics*, **43**, 671-695, 2005.
- [4] L. Auersch, The effect of critically moving loads on the vibrations of soft soils and isolated railway tracks. *Journal of Sound and Vibration*, **310**, 587-607, 2008.
- [5] L. Auersch, Train induced ground vibrations – different amplitude-speed relations for different layered soils. *Journal of Rail and Rapid Transit*, submitted 2010.
- [6] L. Auersch, M. Maldonado, Interaction véhicule-voie-sol et vibrations dues aux trains: modélisations et vérifications expérimentales. *Revue Européenne de Mécanique Numérique*, submitted 2009.
- [7] L. Auersch, S. Said, W. Rücker, *Das Fahrzeug-Fahrweg-Verhalten und die Umgebungerschütterungen bei Eisenbahnen*. Forschungsbericht 243, BAM, Berlin, 2001.
- [8] K. Liu, *Analysis and monitoring of dynamic effects of train-bridge interaction*. PhD Thesis, KU Leuven, 2010.
- [9] M. Martínez Rodrigo, *Atenuación de vibraciones resonantes en puentes de ferrocarril de alta velocidad mediante amortiguadores fluido-viscosos*. PhD Thesis, Universidad Politecnica, Valencia, 2009.

- [10] L. Auersch, Ground vibration due to railway traffic - The calculation of the effects of moving static loads and their experimental verification. *Journal of Sound and Vibration*, **293**, 599-610, 2006.
- [11] UIC Code 776-2: *Design requirements for rail-bridges based on interaction phenomena between train, track and bridge*. 2009

APPENDIX A - MEASURED COMPLIANCES OF THE DIFFERENT TRACKS

The compliances of the different tracks of the surface, bridge and tunnel line have been measured by impulse tests and are shown on Figure 10 for a wide frequency range. The slab track in the tunnel has a high compliance up to 200 Hz (Fig. 10c) whereas the ballasted tracks drop down below 100 Hz (Figs. 10a and b). The bridge and tunnel track show a resonance, the ballasted track on the soil has no resonance amplification. The slab track in the tunnel has two resonances, the strongest at 205 Hz is due to the rail mass on the rail pad stiffness, and the minor resonance at about 100 Hz is due to the plate mass on the sub-soil stiffness. The displacements of the rail on the medium soft rail pad are ten times higher than those of the plate (Fig. 10c). The sleeper to rail amplitude ratios of the ballasted tracks are at about 70 %. All these details are in agreement with the theoretical results.

The experimental results can be used to choose the ballast and sub-soil parameters. The low-frequency decay of the ballasted tracks means a low stiffness of the ballast during the impulse tests. A higher stiffness of the ballast is expected under train loading. The sub-soil stiffness in the tunnel is stiff, but a thinner layer or a thinner plate could also explain the high plate-subsoil resonance frequency.

APPENDIX B – MEASURED TRAIN PASSAGE OVER THE DIFFERENT TRACKS

The behaviour of the different tracks under train passages is shown in Figure 11. The time histories on the left show the displacements of the rail and the sleeper which are calculated from the measured velocities [3]. The third of octave spectra on the right are for the original velocity measurements and compare several rail, sleeper and environmental measuring points. The displacements under a 100 kN axle load is about 0.3 mm for the ballasted track. The displacement of the slab track with softer rail pads are somewhat higher, but the displacements of the plate are considerably smaller as can be observed at the time histories and the spectra.

APPENDIX C – MEASURED TRAIN PASSAGE OVER THE BRIDGE

Figure 12 shows the time histories of two train passages over the bridge. One passage is with a train speed of $v_T = 100$ km/h, the other with $v_T = 160$ km/h. The time segment, when the middle of the train passes the bridge, is selected. A clear resonance is observed for both passages. For the lower train speed, all measuring points on the bridge are in phase, so it is a first symmetric mode of the bridge. For the higher train speed the north and south end of the bridge are in anti-phase and the middle of the bridge has the lowest amplitude. That means that a second antimetric mode is excited by the train at 160 km/h. The eigenfrequencies which are clearly dominating for each train passage are also different, $f = 7$ Hz for $v_T = 100$ km/h and $f = 11$ Hz for $v_T = 160$ km/h.

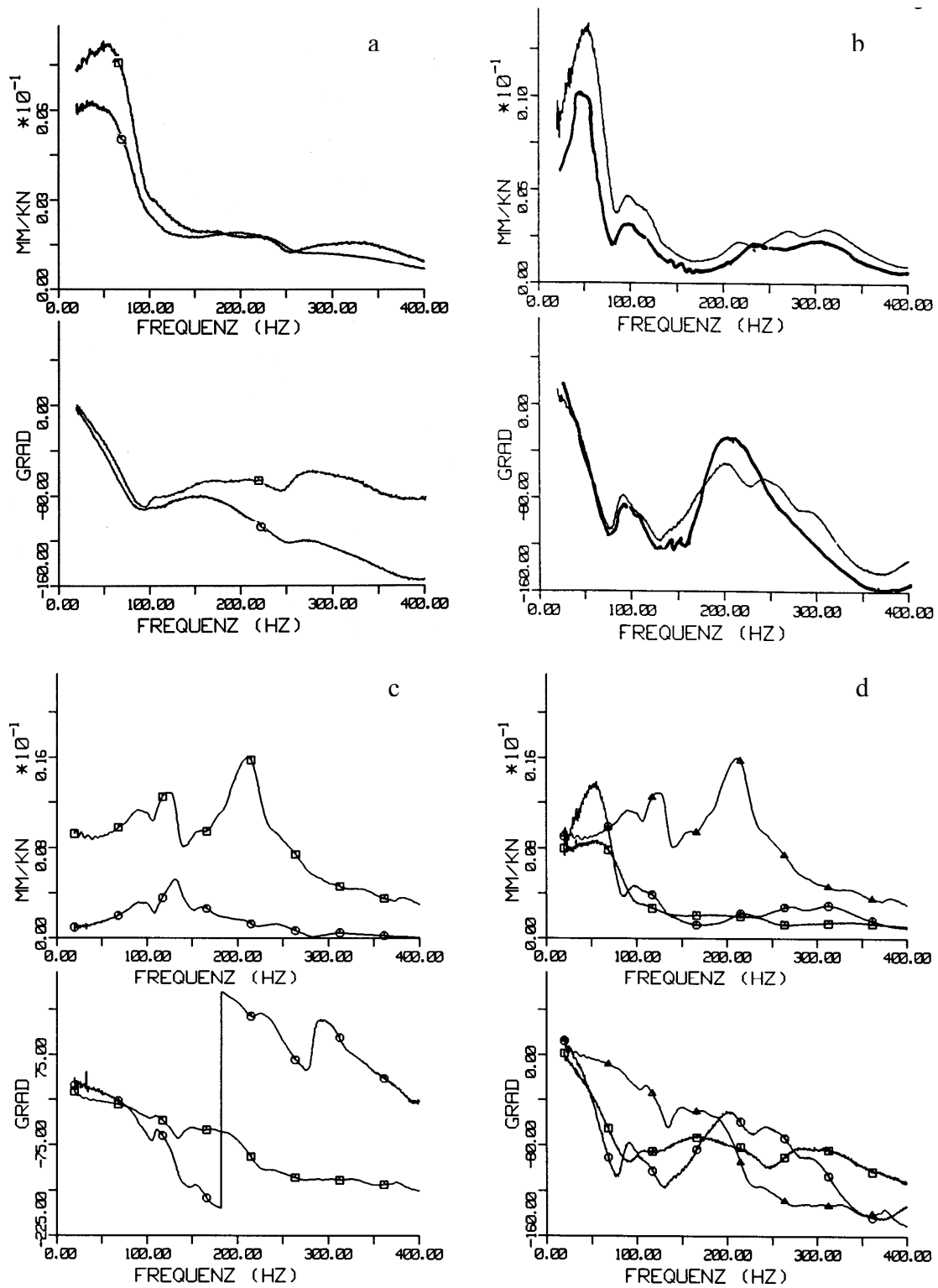
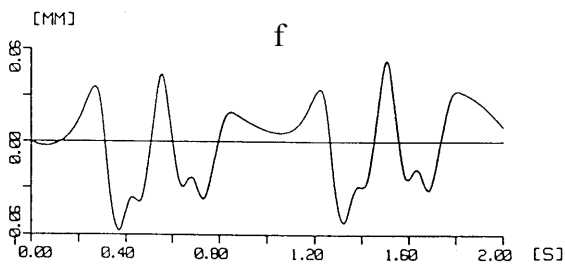
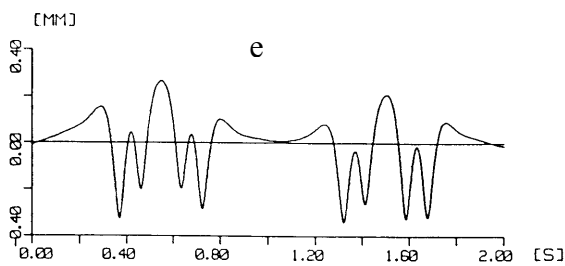
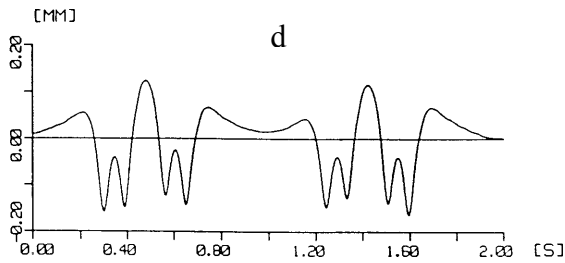
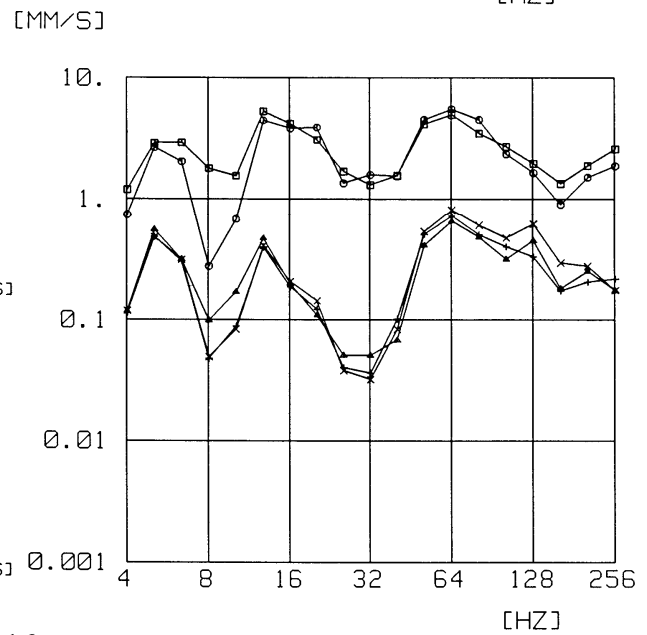
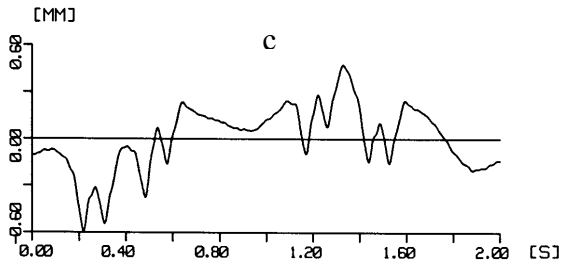
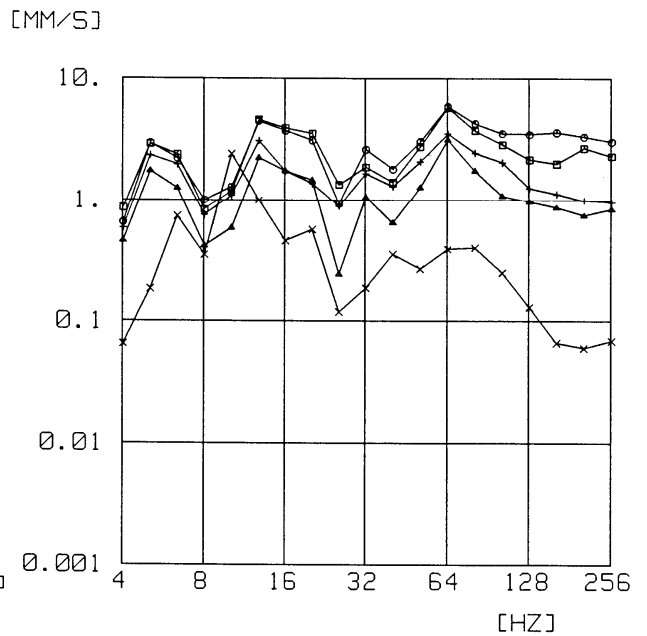
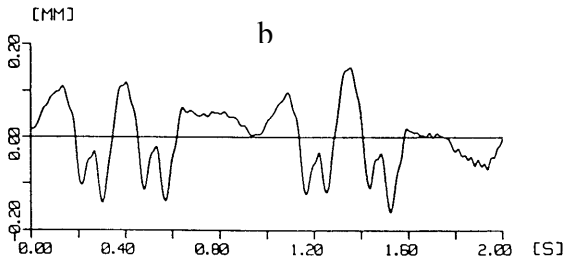
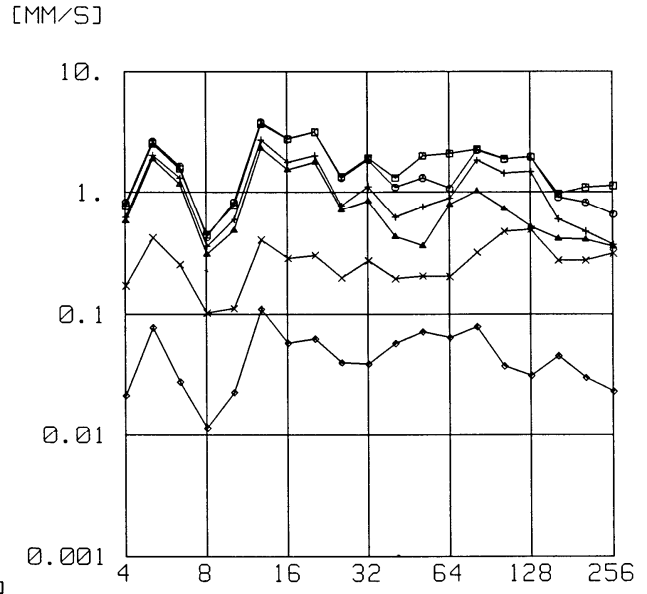
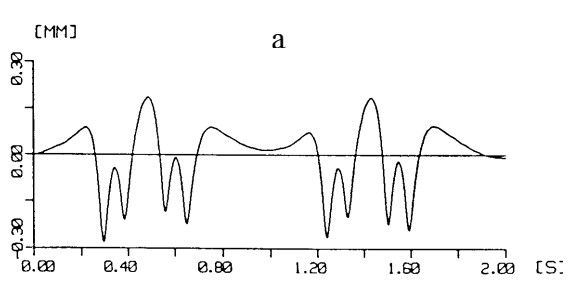


Figure 10: Compliances of the rail (\square) and sleeper (\circ) of the different tracks, a) on the soil, b) on the bridge, c) in the tunnel, d) comparison of the rail compliance for the ballasted track \square on the soil, \circ on the bridge, and \triangle the slab track in the tunnel.



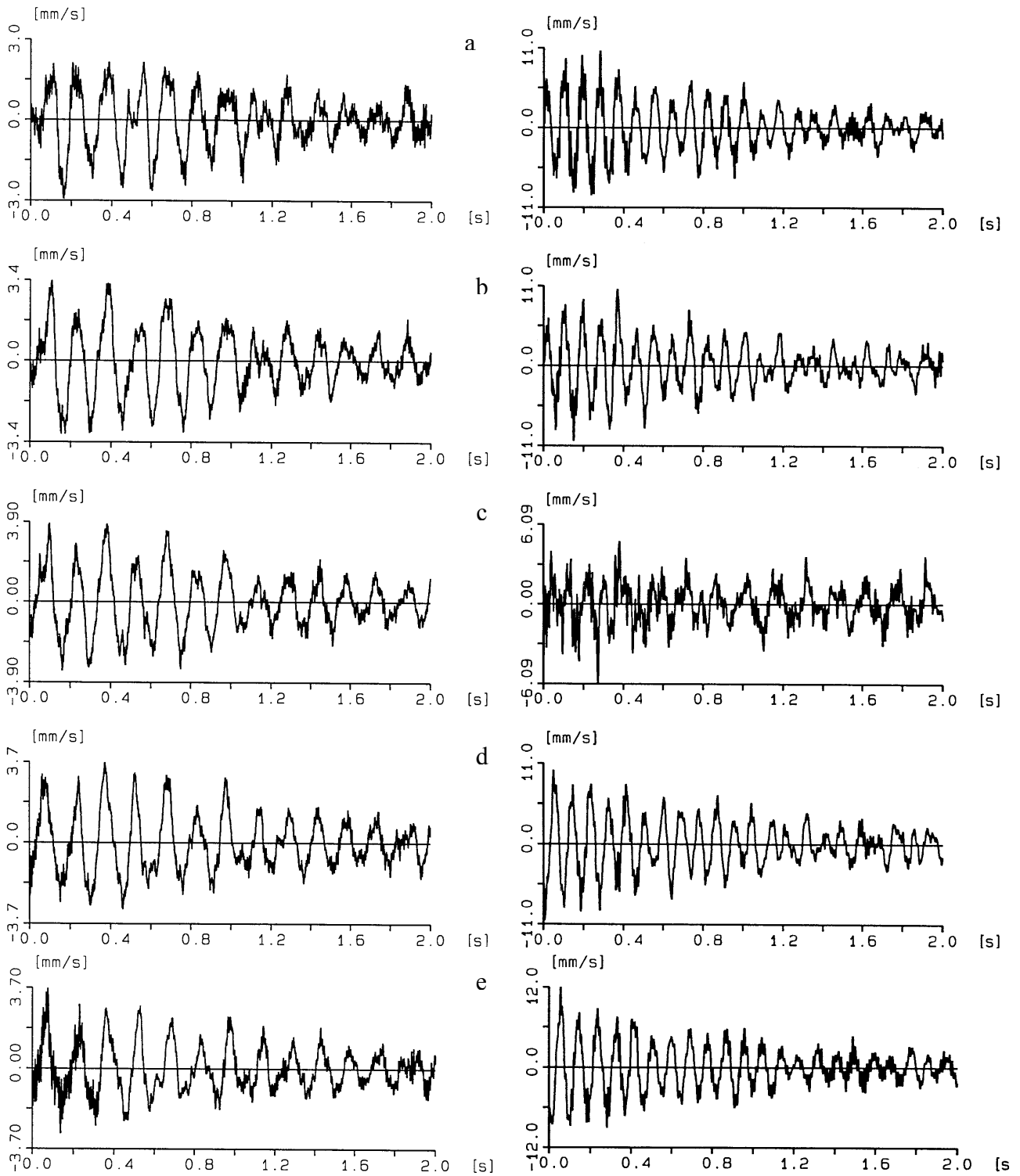


Figure 12: Time histories of the passage of the train with $v_T = 100$ km/h (left) and 160 km/h (right) at $x =$ a) 7.5, b) 15, c) 22.5, d) 30, e) 37.5 m

Figure 11 (previous page): Passage of the train over the different tracks surface line (top), bridge (middle) and tunnel (bottom), time histories of the displacements of the rail (a, c, e) and the sleeper (b, d, f), third-of octave spectra of the rail (\square , \circ), the sleeper (\triangle , $+$) and the soil, bridge or plate (\times).